

Introverted Brønsted acid cavitands for selective conjugate addition reactions

Yasuhiro Matsumoto, Yuta Taguchi, Naruhiro Yoshida, Shugo Tokai,
Tomoyuki Maruyama & Tetsuo Iwasawa

To cite this article: Yasuhiro Matsumoto, Yuta Taguchi, Naruhiro Yoshida, Shugo Tokai, Tomoyuki Maruyama & Tetsuo Iwasawa (2021): Introverted Brønsted acid cavitands for selective conjugate addition reactions, *Supramolecular Chemistry*, DOI: [10.1080/10610278.2021.1981323](https://doi.org/10.1080/10610278.2021.1981323)

To link to this article: <https://doi.org/10.1080/10610278.2021.1981323>

 [View supplementary material](#) 

 Published online: 29 Oct 2021.

 [Submit your article to this journal](#) 

 [View related articles](#) 

 [View Crossmark data](#) 



Introverted Brønsted acid cavitands for selective conjugate addition reactions

Yasuhiro Matsumoto, Yuta Taguchi, Naruhiro Yoshida, Shugo Tokai, Tomoyuki Maruyama and Tetsuo Iwasawa 

Department of Materials Chemistry, Ryukoku University, Otsu, Japan

ABSTRACT

Four new quinoxaline-spanned cavitands having a diester hydrogen phosphate group were successfully synthesised. These phosphorous derivatives were applied in Brønsted acid-assisted catalytic conjugate addition reactions. The results were ranked with the control of diphenyl hydrogen phosphate as well as among those four cavitands. The structure–activity relationship revealed that the catalyst centre surrounded by two *trans*-positioned quinoxalines significantly influences reaction profile and product distribution. This comparative study provides us an intellectual basis for future catalytic cavitand chemistry and artificial enzymatic catalysis.

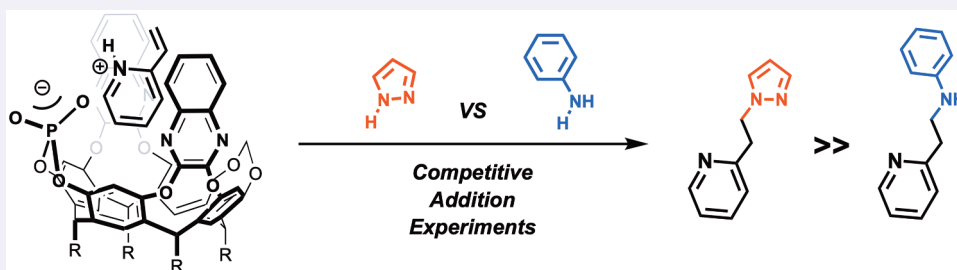
ARTICLE HISTORY

Received 22 June 2021

Accepted 12 September 2021

KEYWORDS

Brønsted acids; introverted functionality; supramolecular catalysis; cavitands; artificial enzymes



Introduction

Mother Nature has been meticulously crafting enzymes for some four billion years, and the transformations they perform are the ultimate inspiration for any catalytic endeavour we make [1–3]. Many distinct structural features are identifiable: 1) the host must provide the guest with a pocket so that encapsulation through host–guest interactions can occur, 2) an inwardly directed reactive centre must be present. These two salient features give rise to specialised transformations that are necessary for life [4,5]. The pocket and the guest are dynamic and move, making adjust for optimisation of binding, reaction, and departure.

From our synthetic point of view, these features can be explored using supramolecular cavitands[6]. The cavitand architecture has evolved over a much shorter time period, but human ingenuity gives us the advantage of semi-rational design of cavitand platforms, the common platforms where our attention is drawn contain curvature⁷ calixarenes[8], cyclodextrins[9], cyclotrimeratrylenes[10], and resorcinarenes[11]. However, inward orientation of reaction centres towards the cavity has been underdeveloped owing to synthetic difficulties.

When the reactive moiety is installed into the cavitand, we often face the problem that products consist of in- and out-ward functionalised isomers[12].

Our recently reported quinoxaline-walled resorcin[4]arene cavitand provided us an opportunity to instal reactive functional groups pointing inwardly. For example, one side AuCl serves as an activator for alkynes, and on the other P = O works as a hydrogen bond acceptor, luring water into the close spatial proximity[13]. In other examples, a bis-AuCl cavitand brings two alkynes together to result in a dimerisation event[14]. Looking down below each cavitand, we see the concave resorcin[4]arene, providing a definite hollow. This hollow has limited space in which transition-state geometry and reaction intermediate are actively stabilised; thus, highly regio-selective transformations unthinkable so far are achieved. The efficient reactions are otherwise daunting: typical catalytic ligands do not provide a platform to control the reaction selectivity and efficiency. We do not think these arrangements are the only possibilities for functionalising cavitands, as other introvertedly catalytic functionality can be attached to the peripheral positions.

In this work, we remove the metal and explore the capabilities of cavitands that position a Brønsted acid of a diaryl hydrogen phosphate moiety (Figure 1)[15]. The acid **1** is flanked by three quinoxaline-walls those arrange for a definite compartment. The chemical cavity in **2** and **3** is loosely screened off from the bulk solution by *cis*- and *trans*-positioned two quinoxaline-walls, respectively. The

hollow in **4** is partitioned by a single quinoxaline at the rim of a cavitand base. Here, we report syntheses of new introverted Brønsted acids cavitands **1**, **2**, **3**, and **4** those are applicable to catalysts. We anticipated that these four different cavitand-acids would show different catalytic capabilities as well as achieve supramolecular advantages not recognised heretofore.

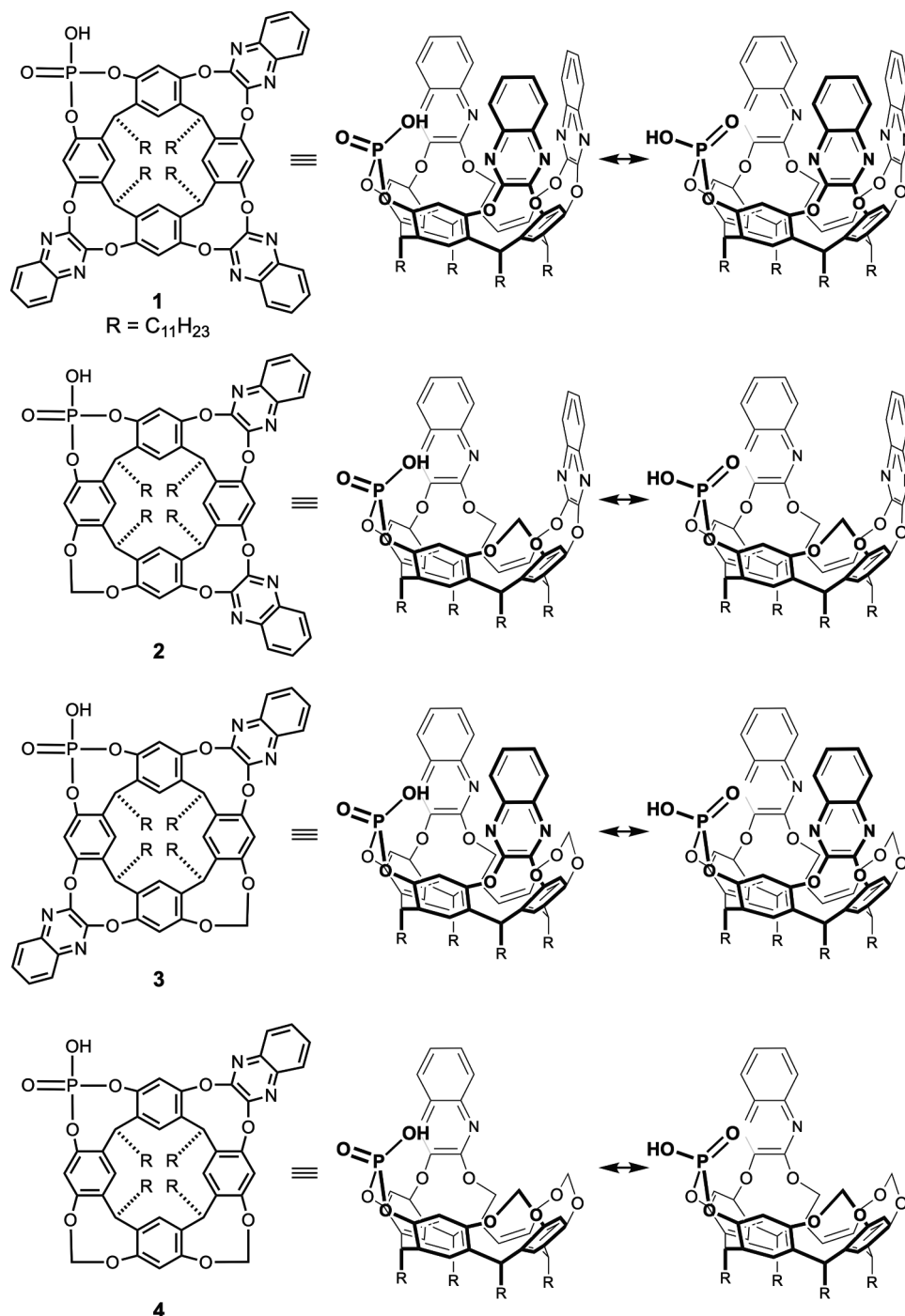


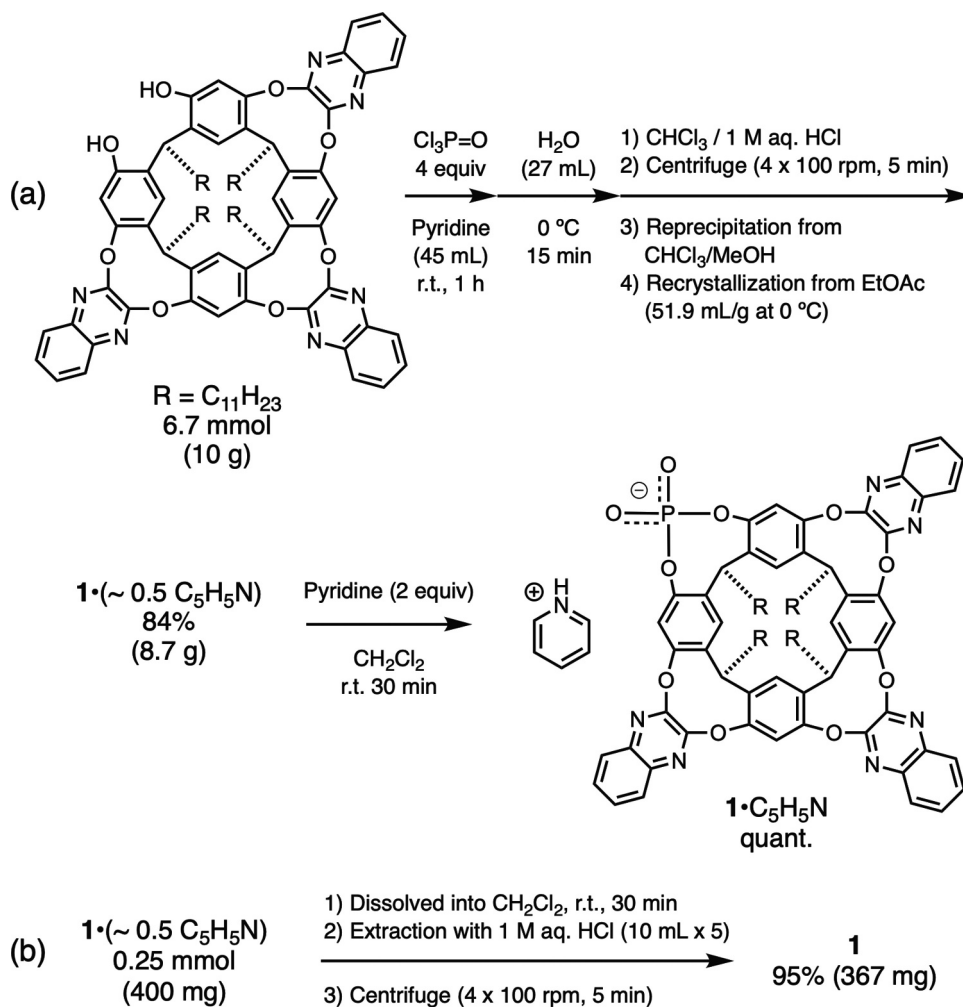
Figure 1. Diaryl hydrogen phosphates **1**, **2**, **3** and **4**.

Results and discussions

Phosphate **1** was derived from a tri-quinoxaline-spanned resorcin[4]arene (Scheme 1)[16]. The starting architecture that structures the diol cavitation formation around its vase-shaped space was previously reported. Upon addition of $\text{Cl}_3\text{P}=\text{O}$ to the diol in pyridine solvent, the reaction smoothly completed in 1 h; however, workup operation caused terrible loss of chemical yields owing to the laborious occurrence of emulsion state. After several attempts, we finally found the procedure described in part (a) of Scheme 1, in which firstly a complex $\mathbf{1}\cdot\text{C}_5\text{H}_5\text{N}$ was produced in high yields with the aid of centrifuge apparatus, reprecipitation, and recrystallisation. Then, part (b) of Scheme 1, extraction of the pyridine of $\mathbf{1}\cdot\text{C}_5\text{H}_5\text{N}$ with 1 M aqueous HCl produced the free acid **1** in 95% yield: the pyridine peaks in the NMR spectra totally disappeared, and the host **1** was surely produced. The molecular structure of $\mathbf{1}\cdot\text{C}_5\text{H}_5\text{N}$ was determined by crystallographic analysis, which clearly disclosed that a singly molecule pyridine resides

inside the compartment in its solid state (Figure 2(a)) [17]. The pyridine is interestingly sandwiched between two quinoxaline walls facing each other, where the hexagonal shape of the pyridine ring almost overlaps with two pyrimidine substructures (Figure 2(b) and (c)). It is especially noteworthy that the pyridine directs the nitrogen atom at the $\text{P}(\text{O})\text{OH}$ moiety (Figure 2(d)). This strongly suggests that an acid-base reaction occurred between the pyridine and $\text{P}(\text{O})\text{OH}$ to give the corresponding salt illustrated in Figure 2(d), which is strongly supported by the nearly same distances between the phosphorus atom and two oxygen atoms (1.469 Å for P1-O9, and 1.474 Å for P1-O10). In addition, the same distance highlights that the phosphate hydrogen in the state of free acid form **1** is not preferentially pointing inward or outward the cavity but it would be fluctuating between the two oxygen groups.

Like as crystallographic analysis, NMR spectroscopic analyses of $\mathbf{1}\cdot\text{C}_5\text{H}_5\text{N}$ for a solution state also explained that one pyridine molecule is folded inside



Scheme 1. Synthesis of (a) a pyridinium salt $\mathbf{1}\cdot\text{C}_5\text{H}_5\text{N}$, and (b) a free acid **1** through extraction of the interior pyridine

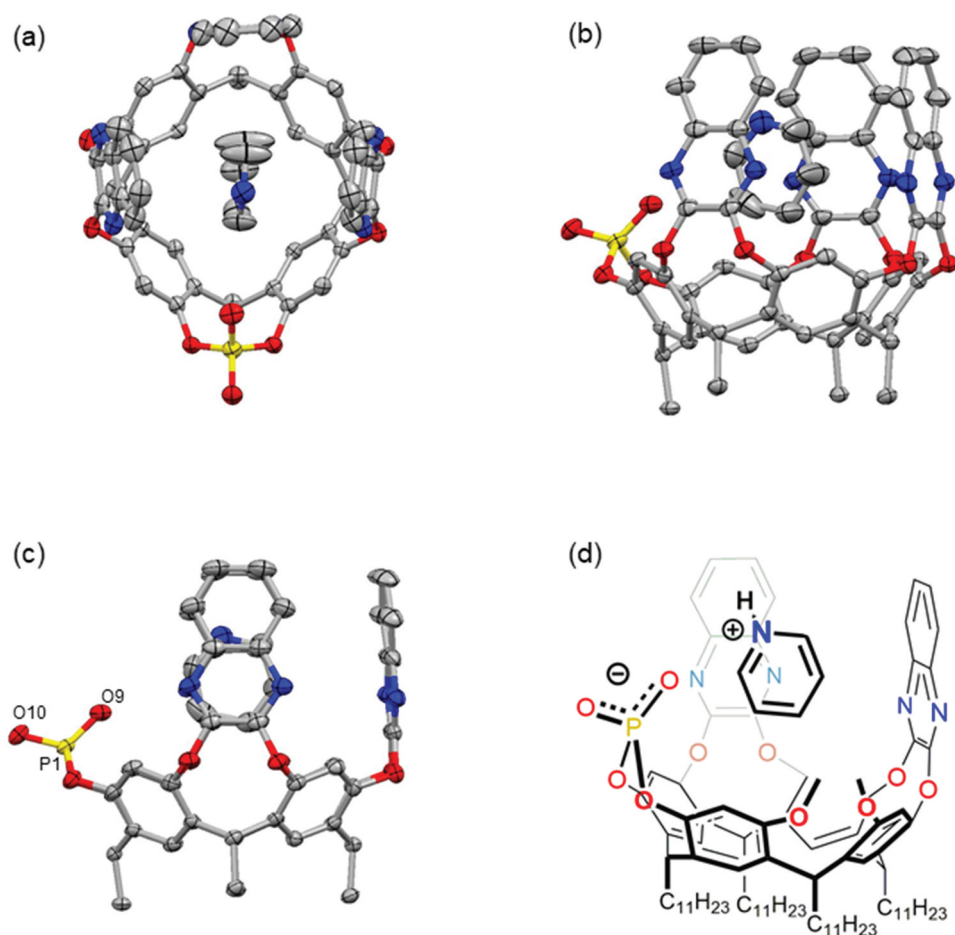


Figure 2. ORTEP drawing of **1**·C₅H₅N with thermal ellipsoids at the 50% probability level; (a) top view; (b) side view from a gap between two quinoxaline moieties; (c) side view from a quinoxaline wall; (d) an illustration for **1**·C₅H₅N where a quinoxaline moiety standing in the foreground was omitted for ease of viewing. Blue for nitrogen atoms, red for oxygen atoms, and yellow for phosphorous atoms. A pyridine molecule resides inside the cavity hollow. The hydrogen atoms are omitted for clarity. Selected bond lengths [Å]: 1.469 for P1-O9, and 1.474 for P1-O10.

the space: three kinds of pyridine proton peaks in ¹H NMR (400 MHz, CD₂Cl₂) are located at 5.58, 4.70 and 4.14 ppm (Figure S1)[18]. These three peaks are not sharp, but each integral value is properly 2:1:2, which strongly suggest each peak corresponds to 2-, 4-, and 3-positioned protons of one interior pyridine (Figure S1)[19].

Further ¹H NMR-analyses in deuterated solvents those are CD₂Cl₂, C₆D₆, C₇D₈, *para*-C₈D₁₀, and 1,3,5-C₉D₁₂ unveiled differences between the host-guest complex **1**·C₅H₅N and free acid **1** (Figure 3). The spectra of **1**·C₅H₅N showed clear peaks those are rationally assigned. For example, the spectra in C₆D₆, C₇D₈, *para*-C₈D₁₀, and 1,3,5-C₉D₁₂ were shown in part (a), (b), (c) and (d): three kinds of methine protons directly below three quinoxaline walls appear sharply at around 5.5–6.5 ppm (marked with squares), which means vase conformers are predominantly formed in these solvents[20]. The acid and base pair would be tightly interacted, so the interior pyridine

ring unwaveringly stayed on. On the other hand, for free **1**, the spectra in CD₂Cl₂ and C₆D₆ showed definite peaks, yet in C₇D₈, *para*-C₈D₁₀, and 1,3,5-C₉D₁₂ gave numerous small, obscure, and broad signals in part (f), (g), and (h): many protons including the methine protons directly below three quinoxaline walls were not settled (marked with triangles). This suggests that conformations of **1** in C₇D₈, *para*-C₈D₁₀, and 1,3,5-C₉D₁₂ float between the vase and kite forms and/or drift with molecular interaction of dimerisation owing to the cavity non-full of these aromatic solvents.

Does the inside space of **1** mismatch a molecule C₇D₈, *para*-C₈D₁₀, and 1,3,5-C₉D₁₂ for reasons of size adjustment or functional complementarity? So, we had fitting experiments of 2-picoline and 2,4,6-collidine because these two molecules are similar size and shape to C₇D₈ and 1,3,5-C₉D₁₂ (Figure 4). To the flask charged with free acid **1** in C₇D₈ was added 1.2 equiv of 2-picoline or 2,4,6-collidine, which gave sharp and reasonable peaks along with

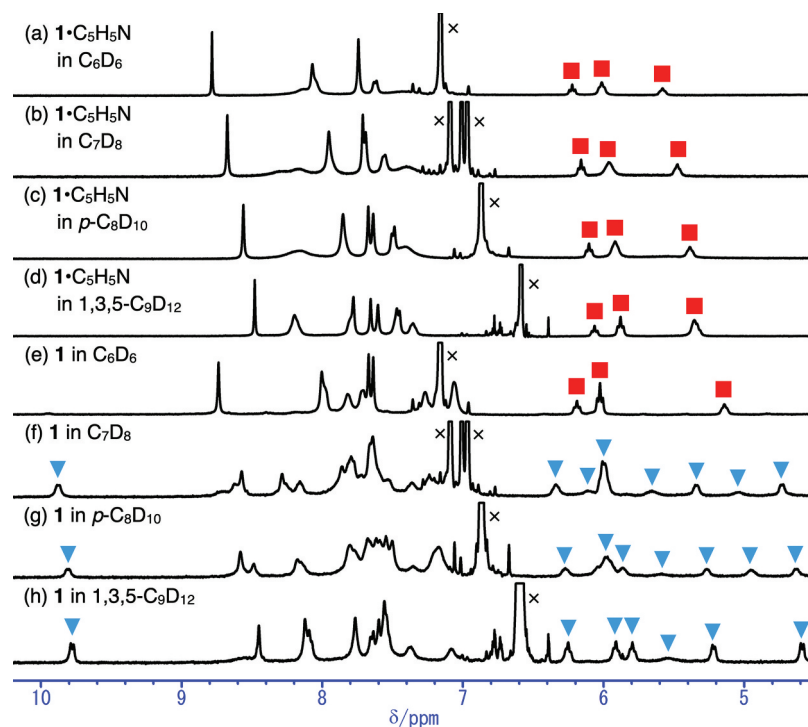


Figure 3. Portions of the ^1H NMR spectra (400 MHz, 298 K) of (a) $1\cdot\text{C}_5\text{H}_5\text{N}$ in C_6D_6 ; (b) $1\cdot\text{C}_5\text{H}_5\text{N}$ in C_7D_8 ; (c) $1\cdot\text{C}_5\text{H}_5\text{N}$ in $p\text{-C}_8\text{D}_{10}$; (d) $1\cdot\text{C}_5\text{H}_5\text{N}$ in $1,3,5\text{-C}_9\text{D}_{12}$; (e) **1** in C_6D_6 ; (f) **1** in C_7D_8 ; (g) **1** in $p\text{-C}_8\text{D}_{10}$; (h) **1** in $1,3,5\text{-C}_9\text{D}_{12}$. ■: methine protons directly below three quinoxaline moieties, ▼: observable but unidentified peaks, X: the residual protons of the deuterated solvents. The spectra of part (a)–(e) exhibit definite and reasonable signals for vase-shaped complexes, while those of part (f)–(h) gave many small and unidentified peaks.

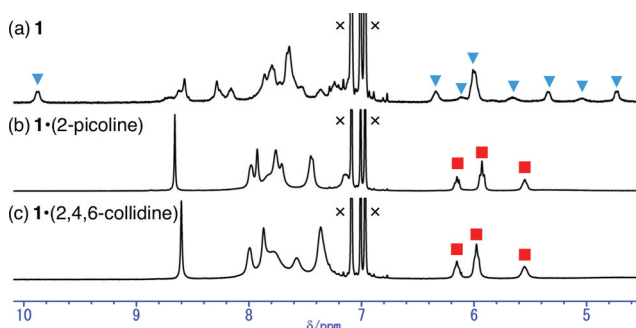
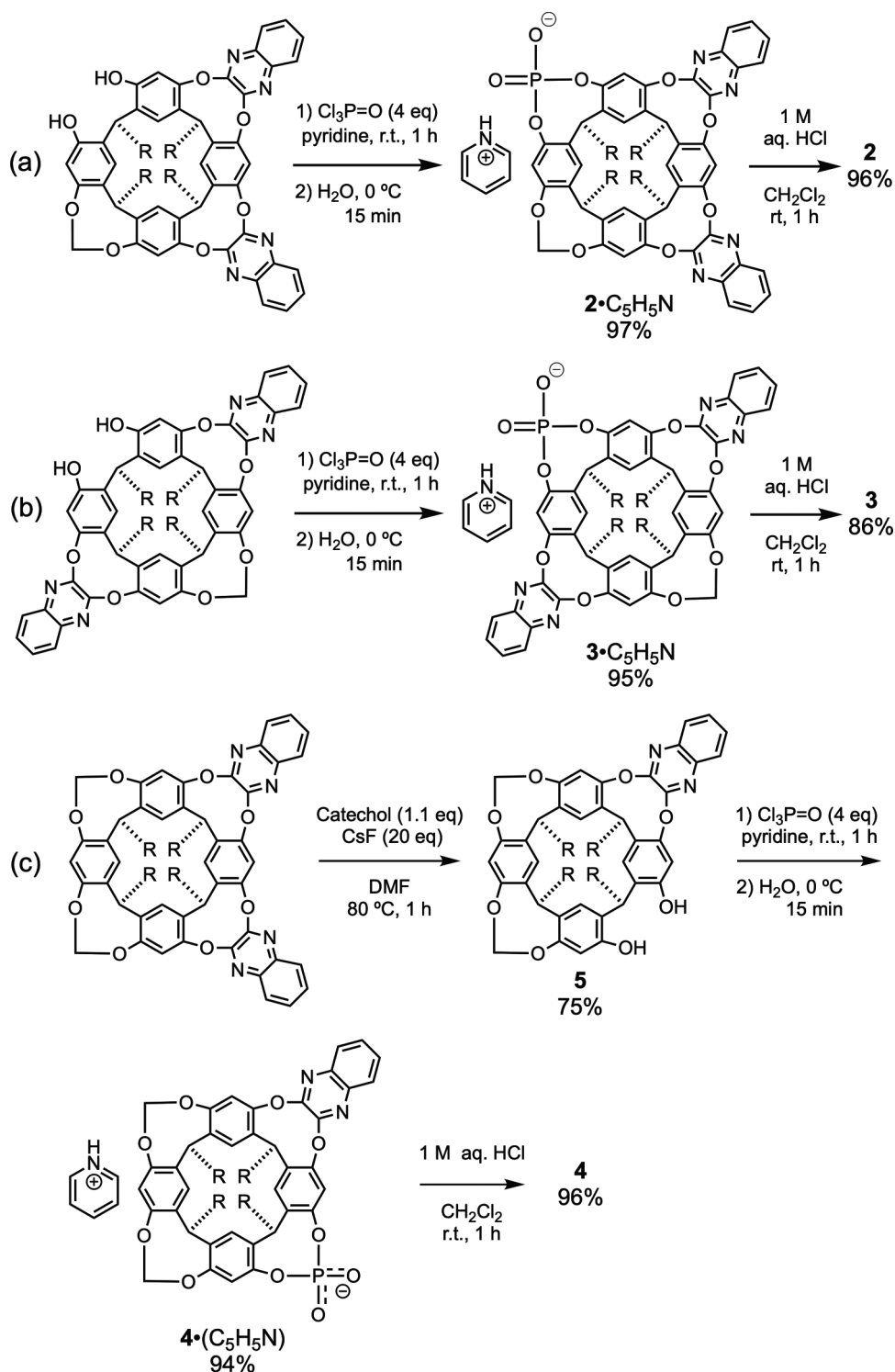


Figure 4. Portions of the ^1H NMR spectra (400 MHz, C_7D_8 , 298 K) of (a) **1**; (b) $1\cdot(2\text{-picoline})$; (c) $1\cdot(2,4,6\text{-collidine})$. ■: methine protons directly below three quinoxaline moieties, ▼: observable but unidentified peaks, X: the residual protons of the deuterated solvents. The spectrum of part (a) shows many small and unidentified peaks, and those of part (b) and (c) exhibit definite and reasonable signals for vase-shaped complexes.

straightforward assignments (part (b) and (c)) as compared to the unclear methine peaks of free **1** in C_7D_8 (part (a)). These explain that 2-picoline and 2,4,6-collidine were forcibly and definitely encapsulated through the acid-base pair. Therefore, the analogously shaped toluene and mesitylene were not too over-sized to fit inside, and

the electronically more neutral toluene and mesitylene than 2-picoline and 2,4,6-collidine are less compatible with the interior space[21].**

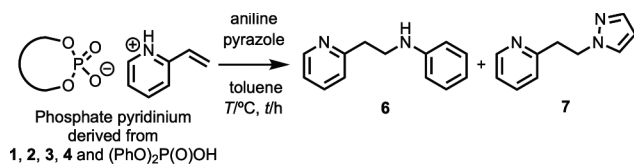
Next, we synthesised the two walls derivatives displaying the aromatic panels in adjacent and opposed orientations according to the preparative procedure of **1** (Scheme 2(a) and (b)). The starting di-quinoxaline-spanned resorcin[4]arene diols were previously reported [16,22]. The high-yielding transformation of the diols into the corresponding $2\cdot\text{C}_5\text{H}_5\text{N}$ and $3\cdot\text{C}_5\text{H}_5\text{N}$ succeeded, and the following removal of the pyridine guest by addition of 1 M aqueous HCl produced the free acids **2** and **3**. We also prepared the single wall derivative displaying the aromatic panel in an adjacent position (Scheme 2(c)). The starting cavitand bearing two quinoxalines and two bridged-methylenes, that is previously reported [22], underwent removal of just single quinoxaline group to yield **5** in 75%. A reaction between **5** and $\text{Cl}_3\text{P}=\text{O}$ afforded $4\cdot\text{C}_5\text{H}_5\text{N}$, and the following extraction of the pyridine provided free acid **4** in 94% yield. These three free acids in C_7D_8 , $p\text{-C}_8\text{D}_{10}$, and C_9D_{12} as well as CD_2Cl_2 and C_6D_6 afforded clear ^1H NMR spectra with reasonable assignments. This indicates that the free acids **2**, **3**, and **4** readily encapsulate C_7D_8 , $p\text{-C}_8\text{D}_{10}$, and C_9D_{12} .



Scheme 2. Synthesis of (a) **2** and **2·C₅H₅N**; (b) **3** and **3·C₅H₅N**; (c) **4** and **4·C₅H₅N**.

When it is compared **1**, **2**, **3**, and **4** to **1·C₅H₅N**, **2·C₅H₅N**, **3·C₅H₅N**, and **4·C₅H₅N** from the view point of compound stability, free acids **1–4** were much more labile than pyridinium salts **1·C₅H₅N**, **2·C₅H₅N**, **3·C₅H₅N**, and **4·C₅H₅N**. One of the problems associated with the free acids lies in their strong acidity^[23] The white solid materials **1–4** observably

decomposed in around one week after purification, changing colour to the reddish samples with multiple spots in TLC analysis. On the other hand, **1·C₅H₅N**, **2·C₅H₅N**, **3·C₅H₅N**, and **4·C₅H₅N** did not decompose even one year after. Thus, we kept **1·C₅H₅N**, **2·C₅H₅N**, **3·C₅H₅N**, and **4·C₅H₅N** in storage and prepared **1–4** right before we used them.



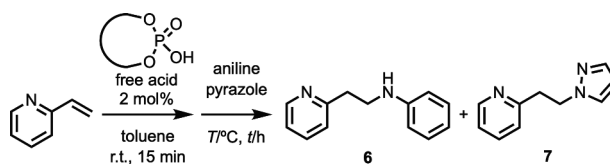
Scheme 3. Competitive conjugate addition of aniline and pyrazole to the complex phosphate (2-vinyl)pyridinium to form **6** and **7**.

In seeking to develop a reactivity profile of **1–4** we made plans to carry out competitive conjugate addition reactions between the nucleophilic reagents, and then decided to employ aniline and pyrazole (Scheme 3). We allocated the Michael acceptor to (2-vinyl)pyridine that was activated by diaryl hydrogen phosphate of a free-acid cavitand (**1–4**) or a control (PhO)₂P(O)OH[24]. These phosphate pyridinium complex between the (2-vinyl)pyridine and diaryl hydrogen phosphate was ensured in ¹H NMR spectra, and the isolated complexes were employed (Figure S2)[25]. Results in the competitive experiments were summarised in Table 1. For entries 1 and 2, the reaction didn't occur in the absence of protic acid. For entries 3 and 4, the presence of (PhO)₂P(O)OH facilitated the addition to yield **6** as a major adduct in around 70% and **7** as a minor adduct in around 10%[26]. When the temperature rose to 45°C, the reaction time got much shorter to 5 h (entry 4). For entries 5 and 6, cavitand **1** was used: In contrast to the control (PhO)₂P(O)OH, the reaction time was prolonged owing to the steric hindrance, and the gap in chemical yields between **6** and **7** was greatly narrowed (entry 6). For entries 7–10, when two-walled cavitands **2** and **3** were applied, the major and minor products were totally reversed. Chemical yields of **6** were gradually decreasing and those of **7** were slowly increasing: Finally, in entry 10, the adduct **6** was a minor product in 19% yield, and

Table 1. Evaluation of product distribution in reactions conducted via Scheme 3.^[a]

| Entry | Phosphate Pyridinium | T/°C | t/h ^[b] | %Yield ^[c] | |
|-------|---|------|--------------------|-----------------------|----|
| | | | | 6 | 7 |
| 1 | none | r.t. | 20 | 0 | 0 |
| 2 | none | 45 | 14 | 0 | 0 |
| 3 | (PhO) ₂ P(O)OH·C ₇ H ₇ N | r.t. | 30 | 66 | 10 |
| 4 | (PhO) ₂ P(O)OH·C ₇ H ₇ N | 45 | 5 | 72 | 12 |
| 5 | 1 ·C ₇ H ₇ N | r.t. | 72 | 61 | 9 |
| 6 | 1 ·C ₇ H ₇ N | 45 | 24 | 41 | 33 |
| 7 | 2 ·C ₇ H ₇ N | r.t. | 48 | 29 | 40 |
| 8 | 2 ·C ₇ H ₇ N | 45 | 20 | 29 | 42 |
| 9 | 3 ·C ₇ H ₇ N | r.t. | 24 | 25 | 46 |
| 10 | 3 ·C ₇ H ₇ N | 45 | 12 | 19 | 52 |
| 11 | 4 ·C ₇ H ₇ N | r.t. | 24 | 34 | 35 |
| 12 | 4 ·C ₇ H ₇ N | 45 | 14 | 32 | 38 |

[a] Conditions: phosphate pyridinium (0.30 mmol), aniline (0.080 mL, 0.90 mmol), pyrazole (61 mg, 0.90 mmol), toluene (1.2 mL). [b] Reactions were stopped when (2-vinyl)pyridine was consumed. [c] Isolated yields after silica-gel column chromatography



Scheme 4. Acid-catalysed competitive addition reactions of aniline and pyrazole to (2-vinyl)pyridine to form **6** and **7**.

major adduct **7** was predominantly formed in 52%. For entries 11 and 12, the single-walled **4** provided mostly same yields for **6** and **7**: the production capability of **4** seems to be between **1** and **2**. Thus, the distribution of **6** and **7** was strongly affected by structural difference in quinoxalines-organised architectures.

In a similar vein, catalytic performance of **1–4** was also studied, according to the Scheme 4. First, the Michael acceptor of (2-vinyl)pyridine incorporated with 2 mol% of diaryl hydrogen phosphate: then, two Michael donors of aniline and pyrazole were added. Results were summarised in Table 2. Reactions at room temperature were sluggish, remaining unreacted (2-vinyl)pyridine (entries 1, 3, 5, 7, 9, 11). On the other hand, reactions at 45°C completed and the gaps in chemical yields between **6** and **7** were narrowed in the order of (PhO)₂P(O)OH, **1**, **2**, and **3** (entries 4, 6, 8, 10). The production capability of **4** seems to be close to that of **2** (entries 11 and 12).

Given the structure–activity relationship in Tables 1 and 2, a mix of tall quinoxalines and small bridging-methylenes has turned out to be potent strategy for the preferential production of **7**. The important thing is that the well-arranged two-quinoxalines in *trans*-position present the cavity with remarkable reactivity and selectivity: the three quinoxalines are oversupply and one wall is in short supply. Very likely, this will arrive at

Table 2. Evaluation of acid capabilities in catalytic reactions conducted via Scheme 4.^[a]

| Entry | Diaryl Hydrogen Phosphate | T/°C | t/h ^[b] | %Yield ^[c] | | |
|-------|---------------------------|------|--------------------|-----------------------|-----|-------------------|
| | | | | 6 | 7 | (2-vinyl)pyridine |
| 1 | none | r.t. | 20 | 0 | >99 | |
| 2 | none | 45 | 14 | 0 | >99 | |
| 3 | (PhO) ₂ P(O)OH | r.t. | 46 | 55 | 16 | |
| 4 | (PhO) ₂ P(O)OH | 45 | 24 | 65 | 22 | |
| 5 | 1 | r.t. | 90 | 49 | 13 | |
| 6 | 1 | 45 | 90 | 51 | 33 | |
| 7 | 2 | r.t. | 90 | 49 | 10 | |
| 8 | 2 | 45 | 54 | 45 | 32 | |
| 9 | 3 | r.t. | 90 | 39 | 14 | |
| 10 | 3 | 45 | 48 | 47 | 43 | |
| 11 | 4 | r.t. | 90 | 43 | 13 | |
| 12 | 4 | 45 | 48 | 48 | 32 | |

[a] Conditions: diaryl hydrogen phosphate (0.020 mmol), (2-vinyl)pyridine (0.11 mL, 1.0 mmol), aniline (0.27 mL, 3.0 mmol), pyrazole (204 mg, 3.0 mmol), and toluene (1.2 mL). [b] Reactions were stopped when (2-vinyl)pyridine was consumed. [c] Isolated yields after silica-gel column chromatography.

a fact that the opened-compartment partitioned by aromatic walls is an important matter in this unusual selective production. Such a molecular architecture would make a difference in chemo-selectivity from flat, plain, and device-less $(\text{PhO})_2\text{P}(\text{O})\text{OH}$ that preferentially forms **6**.

Conclusion

In conclusion, the peripheral hydrogen phosphate in new cavitands **1–4** leads one pyridine guest to its interior space, which provides a new architecture for the chemo-selective transformation and catalysis. This study suggests the following three salient features. Firstly, the preparative syntheses of **1–4** were achieved with crystallographic characterisation of **1**· $\text{C}_5\text{H}_5\text{N}$ complex: Although the acidity is too strong to maintain the framework, the corresponding complex embracing one pyridine molecule is stable enough to stock more than one year. Secondly, the peripheral protic acid regulates entry of a molecule into the cavity hollow which accommodates 2-picoline and 2,4,6-collidine but does not encapsulate similar-sized toluene and 1,3,5-mesitylene. To match inside the narrow space, the basic moiety such as a pyridine core is significant for interaction with the tethered acid and carpeted picloids. Thirdly, a factor essential for the unusual product distribution in the conjugate addition is a mixture of small bridging methylene groups and much taller, flatter quinoxaline groups. The features would be complemented by stabilisation of this chemical processes, which involve nucleophilic attack, de-aromatisation, and re-aromatisation. These are consequences inherent to such a limited space, which has a strong resemblance to enzymatic catalysis that forcibly limits a transition-state geometry and actively stabilise reactive species [27–29]. Although the mechanism resulting in uncommon product distribution is not yet fully known, the presence of introverted Brønsted acid allows us to achieve potent selective transformations and catalysis. Development of a deeper understanding of how this system works, and of new selective transformations, and of new cavitands, is ongoing and will be reported in due course.

Experimental

General methods

All reactions sensitive to air or moisture were carried out under an argon atmosphere and anhydrous conditions unless otherwise noted. Dry solvents were purchased and used without further purification. All reagents were

used as received. Analytical thin layer chromatography was carried out on Merck silica 60F₂₅₄. Column chromatography was carried out with silica gel 60_N (Kanto Chemical Co.). LRMS and HRMS were reported on the basis of TOF (time of flight)-MS (MALDI-TOF or ESI-TOF), and DART (Direct Analysis in Real Time)-MS. ¹H and ¹³C and ³¹P NMR spectra were recorded with a 5 mm QNP probe at 400 MHz and 100 MHz and 162 MHz, respectively. Chemical shifts are reported in δ (ppm) with reference to residual solvent signals [¹H NMR: CHCl_3 (7.26), C_7H_8 (2.08), CH_2Cl_2 (5.32); ¹³C NMR: CDCl_3 (77.0)]. Signal patterns are indicated as s, singlet; d, doublet; t, triplet; q, quartet; m, multiplet; br, broad.

Synthesis of **1**· $\text{C}_5\text{H}_5\text{N}$

(see Scheme 1) Under an argon atmosphere, to a white suspension of tri-quinoxaline-spanned resorcin[4]arene (10 g, 6.7 mmol) in pyridine (45 mL) at room temperature was slowly added POCl_3 (2.47 mL, 27.0 mmol). The starting diol compounds disappeared on TLC monitoring. After stirred for 1 h, the reaction was quenched by addition of water (27 mL) over 5 min at 0°C, and followed by evaporation of all the volatiles. The residue was dissolved in CHCl_3 (90 mL), and 1 M aqueous HCl was added. The resultant emulsion was separated into organic and aqueous phases by centrifuge apparatus (40 × 100 rpm, 5 min). The combined organic phases were dried over Na_2SO_4 , filtered, and concentrated *in vacuo* to give 10.9 g of yellow solid materials as crude products. Reprecipitation from $\text{CHCl}_3/\text{CH}_3\text{OH}$ (1/8, v/v) afforded 10.1 g of white solid materials, and the following recrystallisation from EtOAc (51.9 mL/g) at –5°C yielded white solid of 8.72 g of host-guest complexes that were composed of **1** and pyridine with approximate 1:0.5 ratio. To a colourless solution of the 1:0.5 host-guest complex (1 g, 0.65 mmol) in CH_2Cl_2 (2 mL) at room temperature was added pyridine (0.1 mL, 1.3 mmol). After the mixture was stirred for 30 min, the CH_2Cl_2 solvent and extra amounts of pyridine were evaporated to yield 1 g of **1**· $\text{C}_5\text{H}_5\text{N}$ in 94% as white solid materials. For data of **1**· $\text{C}_5\text{H}_5\text{N}$: *Rf* values 0.46 (toluene/EtOAc, 2:1); ¹H NMR (400 MHz, CDCl_3) 8.26 (s, 2H), 8.03 (m, 2H), 7.69 (m, 4H), 7.56 (d, *J* = 9.0 Hz, 2H), 7.46 (m, 4H), 7.35 (s, 2H), 7.31 (s, 2H), 7.25 (s, 2H), 5.79 (t, *J* = 8.1 Hz, 1H), 5.57 (t, *J* = 8.1 Hz, 2H), 4.98 (t, *J* = 8.1 Hz, 1H), 2.37 (dt, *J* = 8.1, 7.6 Hz, 2H), 2.31 (dt, *J* = 8.1, 7.6 Hz, 2H), 2.23 (dt, *J* = 8.1, 7.4 Hz, 4H), 1.51–1.28 (m, 72 H), 0.90–0.87 (m, 12 H) ppm; ¹³C NMR (100 MHz, CDCl_3) 152.9, 152.6, 152.3, 152.2 (two peaks are overlapped), 152.0, 148.8 (*J*_{CP} = 9.1 Hz), 139.8, 139.3, 139.1, 136.9, 136.5, 135.1, 130.2, 129.9, 129.4, 129.1, 128.1, 127.7, 127.5, 123.3 (two peaks are overlapped), 121.9, 119.3, 118.5, 35.84, 34.00, 32.03

(many peaks are overlapped), 29.84, 29.79, 29.78, 29.50 (many peaks are overlapped), 22.78, 22.76, 14.20, 14.18 (many peaks are overlapped) ppm; ^{31}P NMR (162 MHz, CDCl_3) -17.0 ppm; MS (ESI) m/z : 1626 $[\text{MH}]^+$; IR (neat): 2920, 2848, 1484, 1413, 1330, 1155, 756, 590 cm^{-1} ; HRMS (ESI) calcd. for $\text{C}_{101}\text{H}_{122}\text{N}_7\text{NaO}_{10}\text{P}$: 1649.8984 $[\text{M} + \text{Na}]^+$, found: 1649.8994.

Synthesis of 1

(see Scheme 1) $1 \cdot \text{C}_5\text{H}_5\text{N}$ (400 mg, 0.25 mmol) was dissolved into CH_2Cl_2 (20 mL) at room temperature over 10 min, and the solution was transferred into a 50 mL separatory funnel. The organic phase was washed with 1 M aqueous HCl (10 mL \times 5), and the resultant emulsion was separated into organic and aqueous phases by centrifuge apparatus (40 \times 100 rpm, 5 min). The combined organic phases were dried over Na_2SO_4 , and filtered, and concentrated *in vacuo* to yield 367 mg of free acid **1** (95%) as yellow solid materials. For data of **1**: *Rf* values 0.46 (toluene/EtOAc, 2:1); ^1H NMR (400 MHz, CDCl_3) 8.29 (s, 2H), 7.91 (m, 2H), 7.78 (m, 2H), 7.61–7.59 (m, 4H), 7.53–7.45 (m, 4H), 7.40 (s, 2H), 7.27 (s, 2H), 7.24 (s, 2H), 5.77 (t, $J = 8.2$ Hz, 1H), 5.61 (t, $J = 7.9$ Hz, 2H), 4.90 (t, $J = 6.6$ Hz, 1H), 2.33–2.25 (m, 8 H), 1.44–1.28 (m, 72 H), 0.89 (t, $J = 6.3$ Hz, 12 H) ppm; ^{13}C NMR (100 MHz, CDCl_3) 153.3, 152.9, 152.7, 152.63, 152.59 (two peaks are overlapped), 146.1 (d, $J_{\text{CP}} = 7.4$ Hz), 140.0, 139.9, 137.0, 136.2, 135.6, 134.1 (d, $J_{\text{CP}} = 2.4$ Hz), 129.59, 129.57, 129.2, 128.9, 128.2 (d, $J_{\text{CP}} = 2.2$ Hz), 127.9, 123.5, 122.8, 119.4, 117.1 (d, $J_{\text{CP}} = 3.6$ Hz), 35.95, 34.23, 33.02, 32.10, 32.09, 31.17 (many peaks are overlapped), 29.85, 29.80, 29.59 (many peaks are overlapped), 28.17 (many peaks are overlapped), 14.29 (many peaks are overlapped) ppm; ^{31}P NMR (162 MHz, CDCl_3) -12.3 ppm; MS (MALDI-TOF) m/z : 1548 $[\text{MH}]^+$; IR (neat): 2920, 2849, 1479, 1327, 1157, 1021, 754 cm^{-1} ; HRMS (MALDI-TOF) calcd. for $\text{C}_{96}\text{H}_{118}\text{N}_6\text{O}_{10}\text{P}$: 1547.8714 $[\text{MH}]^+$, found: 1547.8720.

Synthesis of $2 \cdot \text{C}_5\text{H}_5\text{N}$

(see Scheme 2(a)) Under an argon atmosphere, to a white solution of *cis*-di-quinoxaline-spanned resorcin [4]arene (548 mg, 0.4 mmol) in pyridine (5 mL) at room temperature was slowly added POCl_3 (0.15 mL, 1.6 mmol). The starting diol compounds disappeared on TLC monitoring. After stirred for 1 h, the reaction was quenched by addition of water (3 mL) over 5 min at 0°C , and followed by evaporation of all the volatiles. The residue was dissolved in CH_2Cl_2 (10 mL). The organic phase was washed with brine (10 mL \times 2), dried over Na_2SO_4 , filtered, and concentrated *in vacuo* to give 590 mg of white solid materials (97%) as crude products. For

data of $2 \cdot \text{C}_5\text{H}_5\text{N}$: *Rf* values 0.19 ($\text{CH}_2\text{Cl}_2/\text{MeOH}$, 9:1); ^1H NMR (400 MHz, CD_2Cl_2) 8.31 (s, 1H), 8.06 (d, $J = 8.2$ Hz, 1H), 7.94 (d, $J = 8.2$ Hz, 1H), 7.81 (d, $J = 8.2$ Hz, 1H), 7.73–7.55 (m, 5 H), 7.34 (s, 3 H), 7.29 (s, 1H), 7.23 (s, 1H), 7.21 (s, 1H), 7.11 (brs, 2H, 2-positioned protons of the pyridine ring), 6.40 (brs, 2H, including 4-positioned proton of the pyridine ring), 5.95 (brs, 2H, 3-positioned protons of the pyridine ring), 5.75 (t, $J = 8.1$ Hz, 1H), 5.63 (t, $J = 8.1$ Hz, 1H), 5.39 (d, $J = 7.3$ Hz, 1H), 4.84 (t, $J = 7.5$ Hz, 1H), 4.58 (t, $J = 8.0$ Hz, 1H), 3.46 (d, $J = 5.2$ Hz, 1H), 2.36–2.23 (m, 8 H), 1.43–1.28 (m, 72 H), 0.90–0.87 (m, 12 H) ppm; ^{13}C NMR (100 MHz, CD_2Cl_2) 155.9, 155.4 (d, $J_{\text{CP}} = 1.7$ Hz), 153.4, 153.2 (three peaks are overlapped), 153.0, 152.49, 152.45, 152.3 (d, $J_{\text{CP}} = 1.4$ Hz), 149.2 (d, $J_{\text{CP}} = 8.3$ Hz), 148.5 (d, $J_{\text{CP}} = 8.8$ Hz), 142.1, 140.9 (2-positioned carbons of the pyridine ring), 140.2 (two peaks are overlapped), 140.1, 140.0, 139.7, 138.0 (d, $J_{\text{CP}} = 1.8$ Hz), 137.24, 137.18, 137.11, 135.9 (4-positioned carbon of the pyridine ring), 135.5 (two peaks are overlapped), 130.2, 130.1, 129.9, 129.8, 128.5, 128.43, 128.38, 128.3, 124.8 (two peaks are overlapped), 122.9 (3-positioned carbons of the pyridine ring), 122.4, 121.2, 119.2, 118.2 (d, $J_{\text{CP}} = 3.6$ Hz), 117.5, 117.1 (d, $J_{\text{CP}} = 3.4$ Hz), 99.93, 36.84, 36.27, 34.68, 32.38 (many peaks are overlapped), 31.02, 30.18, 29.83 (many peaks are overlapped), 28.43, 23.14, 14.33 (many peaks are overlapped) ppm; ^{31}P NMR (162 MHz, CD_2Cl_2) -17.3 ppm; MS (ESI) m/z : 1512 $[\text{MH}]^+$; MS (ESI) m/z : 1534 $[\text{M} + \text{Na}]^+$; IR (neat) 2922, 2851, 1577, 1486, 1413, 1332, 1161, 968, 751, 602 cm^{-1} ; HRMS (ESI) calcd. for $\text{C}_{94}\text{H}_{120}\text{N}_5\text{NaO}_{10}\text{P}$: 1533.8699 $[\text{M} + \text{Na}]^+$, found: 1533.8675.

Synthesis of 2

(see Scheme 2(a)) $2 \cdot \text{C}_5\text{H}_5\text{N}$ (134 mg, 0.09 mmol) was dissolved into CH_2Cl_2 (10 mL) at room temperature. The solution was transferred into a 50 mL separatory funnel, and the organic phase was washed with 1 M aqueous HCl (10 mL \times 5). The resultant emulsion was separated into organic and aqueous phases by centrifuge apparatus (40 \times 100 rpm, 5 min). The organic phase was dried over Na_2SO_4 , and filtered, and concentrated *in vacuo* to yield 122 mg of free acid **2** (96%) as white solid materials. *Rf* values 0.19 ($\text{CH}_2\text{Cl}_2/\text{MeOH}$, 9:1); ^1H NMR (400 MHz, CD_2Cl_2) 8.28 (s, 1H), 7.96 (brs, 1H), 7.92 (d, $J = 8.4$ Hz, 1H), 7.78 (d, $J = 8.4$ Hz, 1H), 7.75 (brs, 1H), 7.62–7.54 (m, 4 H), 7.40 (brs, 1H), 7.33 (s, 1H), 7.29 (s, 1H), 7.24 (s, 1H), 7.21 (s, 1H), 6.43 (s, 1H), 5.74–5.68 (m, 2H), 5.50 (d, $J = 7.1$ Hz, 1H), 4.68 (t, $J = 8.1$ Hz, 1H), 4.57 (t, $J = 7.1$ Hz, 1H), 4.03 (d, $J = 7.1$ Hz, 1H), 2.34–2.30 (m, 8 H), 1.44–1.27 (m, 72 H), 0.91–0.86 (m, 12 H) ppm; ^{13}C NMR (100 MHz, CD_2Cl_2) 155.8, 153.3, 153.2, 152.95 (two peaks are overlapped), 152.91, 152.8

(two peaks are overlapped), 152.6, 146.4 (d, $J_{\text{CP}} = 6.4$ Hz), 145.9 (d, $J_{\text{CP}} = 6.4$ Hz), 140.3 (two peaks are overlapped), 140.2, 139.7, 138.7, 137.4, 136.8, 136.0, 135.7, 135.2, 133.7, 129.9, 129.8, 129.7, 129.5, 129.4, 128.6, 128.4, 128.3, 128.2, 124.8, 123.6, 122.4, 121.9, 119.3, 117.8, 117.5, 116.61, 116.56, 99.9, 36.9, 36.4, 34.8, 32.7, 32.5, 32.4 (many peaks are overlapped), 31.1, 30.7, 30.3, 30.2 (many peaks are overlapped), 29.9, 28.5, 28.3 (many peaks are overlapped), 23.2, 14.4 ppm; ^{31}P NMR (162 MHz, CD_2Cl_2) -13.3 ppm; MS (ESI) m/z : 1432 $[\text{MH}]^+$; IR (neat) 2913, 2845, 1408, 1324, 1264, 1152, 1013, 961, 754 cm^{-1} ; HRMS (ESI) calcd. for $\text{C}_{89}\text{H}_{116}\text{N}_4\text{O}_{10}\text{P}$: 1431.8429 $[\text{MH}]^+$, found: 1431.8423.

Synthesis of $3\cdot\text{C}_5\text{H}_5\text{N}$

(see Scheme 2(b)) Under an argon atmosphere, to a white solution of *trans*-di-quinoxaline-spanned resorcin[4]arene (480 mg, 0.35 mmol) in pyridine (5 mL) at room temperature was slowly added POCl_3 (0.13 mL, 1.4 mmol). The starting diol compounds disappeared on TLC monitoring. After stirred for 1 h, the reaction was quenched by addition of water (2.5 mL) over 5 min at 0°C , and followed by evaporation of all the volatiles. The residue was dissolved in CH_2Cl_2 (10 mL). The organic phase was washed with brine (10 mL x 2), dried over Na_2SO_4 , filtered, and concentrated *in vacuo* to give 478 mg of yellowish white solid materials (95%) in pure form. For data of $3\cdot\text{C}_5\text{H}_5\text{N}$: *Rf* values 0.32 ($\text{CH}_2\text{Cl}_2/\text{MeOH}$, 9:1); ^1H NMR (400 MHz, CD_2Cl_2): 7.76–7.64 (m, 6 H, including 2-positioned protons of the pyridine ring), 7.58–7.48 (m, 4 H), 7.44 (s, 2H), 7.38 (s, 2H), 7.32 (s, 2H), 7.29 (s, 3 H, including 4-positioned proton of the pyridine ring), 6.17 (brs, 2H, 3-positioned protons of the pyridine ring), 5.87 (d, $J = 7.5$ Hz, 1H), 5.58 (t, $J = 8.1$ Hz, 2H), 5.04 (t, $J = 6.7$ Hz, 1H), 4.88 (t, $J = 8.0$ Hz, 1H), 4.30 (d, $J = 7.2$ Hz, 1H), 2.37–2.25 (m, 8 H), 1.43–1.28 (m, 72 H), 0.92–0.87 (m, 12 H); ^{13}C NMR (100 MHz, CD_2Cl_2) 155.6, 152.7, 152.62, 152.57, 152.4, 149.5 (d, $J_{\text{CP}} = 35.3$ Hz), 144.5 (2-positioned carbons of the pyridine ring), 140.1, 139.8, 139.7, 139.4, 137.0 (4-positioned carbon of the pyridine ring), 136.6, 135.9, 130.0, 129.8, 128.3, 128.2, 124.0, 122.6, 122.4, 118.6 (3-positioned carbons of the pyridine ring), 117.9, 100.2, 54.4, 54.1, 53.6, 37.0, 32.3, 30.1, 29.8, 23.1, 14.3 (many peaks are overlapped) ppm; ^{31}P NMR (162 MHz, CD_2Cl_2) -16.6 ppm; MS (ESI) m/z : 1430 $[\text{M}-\text{C}_5\text{H}_6\text{N}]^-$; IR (neat): 2921, 2849, 1487, 1399, 1328, 1272, 1165, 603 cm^{-1} ; HRMS (ESI) calcd. for $\text{C}_{89}\text{H}_{114}\text{N}_4\text{O}_{10}\text{P}$: 1429.8278 $[\text{M}-\text{C}_5\text{H}_6\text{N}]^-$, found: 1429.8200.

Synthesis of 3

(see Scheme 2(b)) $3\cdot\text{C}_5\text{H}_5\text{N}$ (150 mg, 0.1 mmol) was dissolved into CH_2Cl_2 (20 mL) at room temperature, and the solution was transferred into a 50 mL separatory

funnel. The organic phase was washed with 1 M aqueous HCl (10 mL x 5), dried over Na_2SO_4 , and filtered, and concentrated *in vacuo* to yield 123 mg of free acid **3** (86%) as white solid materials. For data of **3**: *Rf* values 0.32 ($\text{CH}_2\text{Cl}_2/\text{MeOH}$, 9:1); ^1H NMR (400 MHz, CD_2Cl_2): 7.91 (d, $J = 8.0$ Hz, 2H), 7.83 (d, $J = 7.9$ Hz, 2H), 7.63 (s, 2H), 7.56–7.52 (m, 4 H), 7.34 (s, 2H), 7.30 (s, 2H), 7.28 (s, 2H), 5.75–5.68 (m, 3 H), 4.74–4.69 (m, 2H), 4.09 (d, $J = 7.6$ Hz, 1H), 3.80 (brs, 1H), 2.42–2.30 (m, 8 H), 1.46–1.24 (m, 72 H), 0.92–0.84 (m, 12 H) ppm; ^{13}C NMR (100 MHz, CD_2Cl_2) 156.1, 153.0, 152.9, 152.8, 152.5, 146.6, 140.2, 140.1, 139.0, 137.7, 135.4, 134.9, 129.9, 128.4, 128.2, 123.7, 122.6, 117.7, 100.1, 37.0, 36.5, 34.6, 32.4 (many peaks are overlapped), 31.2, 31.1, 30.2 (many peaks are overlapped), 28.4 (many peaks are overlapped), 23.2 (many peaks are overlapped), 14.4 (many peaks are overlapped) ppm; ^{31}P NMR (162 MHz, CD_2Cl_2) -13.4 ppm; MS (ESI) m/z : 1431 $[\text{M}-\text{H}]^-$; IR (neat): 2921, 2849, 1483, 1399, 1328, 1161, 969, 758 cm^{-1} ; HRMS (ESI) calcd. for $\text{C}_{89}\text{H}_{114}\text{N}_4\text{O}_{10}$ P: 1430.8306 $[\text{M}-\text{H}]^-$, Found: 1430.8301.

Synthesis of 5

(see Scheme 2(c)) Under an argon atmosphere, to a solution of the starting di-quinoxaline cavitand (1.4 mg, 1.0 mmol) in DMF (60 mL) at 80°C was added CsF (3.0 g, 20 mmol), and the resultant mixture was followed by addition of a solution of catechol (121 mg, 1.1 mmol) in DMF (11 mL). After the reaction mixture was stirred at 80°C for 1 h, the mixture was cooled to room temperature, and followed by quenching with slow addition of 1 M aqueous HCl (180 mL). The precipitates were filtered off, and washed thoroughly with water (300 mL), and dried up at ambient temperature. The materials were dissolved into CH_2Cl_2 (70 mL), and the solution was washed with brine (20 mL), and dried over Na_2SO_4 , and filtered, and concentrated *in vacuo* to give crude product of 270 mg as brown solid materials. Purification by column chromatography (Toluene/EtOAc = 19:1) afforded **5** of 940 mg as white solid materials (75%). For data of **5**: *Rf* values 0.38 (hexane/EtOAc, 2:1); ^1H NMR (400 MHz, CDCl_3) 7.99–7.96 (m, 2H), 7.69–7.67 (m, 2H), 7.46 (s, 1H), 7.26 (s, 1H), 7.21 (s, 1H), 7.15 (s, 1H), 7.10 (s, 1H), 7.08 (s, 1H), 6.42 (s, 1H), 6.28 (s, 1H), 5.74 (d, $J = 7.2$ Hz, 1H), 5.64 (d, $J = 7.2$ Hz, 1H), 5.58 (t, $J = 8.1$ Hz, 1H), 4.73 (t, $J = 8.1$ Hz, 1H), 4.69 (t, $J = 8.1$ Hz, 1H), 4.32–4.29 (m, 3 H), 2.24–2.22 (m, 8 H), 1.43–1.27 (m, 72 H), 0.90–0.87 (m, 12 H) ppm; ^{13}C NMR (100 MHz, CDCl_3) 155.7, 155.6, 155.2, 155.1, 153.5, 153.1, 152.2, 152.0, 151.8, 151.0, 140.3, 139.3, 139.1, 139.0, 137.8, 135.9, 134.1, 131.2, 130.2 (two peaks are overlapped), 129.4, 128.5, 127.8 (two peaks are overlapped), 125.8, 122.2, 121.9, 120.6, 117.1, 116.9, 110.6, 109.9, 99.9, 99.7,

36.8, 36.3, 34.6, 34.1, 33.7, 32.3 (many peaks are overlapped), 30.8, 30.29, 30.26, 30.2, 30.1 (many peaks are overlapped), 30.0, 29.8 (many peaks are overlapped), 28.4, 28.3, 28.2, 23.1 (many peaks are overlapped), 14.5 (many peaks are overlapped) ppm; MS (ESI) m/z : 1254 [M-H]⁻; IR (neat): 3323, 2921, 2851, 1606, 1579, 1489, 1407, 1331, 957 cm⁻¹; HRMS (ESI) calcd. for C₈₂H₁₁₃N₂O₈: 1253.8502 [M-H]⁻, found: 1253.8520.

Synthesis of 4•C₅H₅N

(see Scheme 2(c)) Under an argon atmosphere, to a solution of **5** (879 mg, 0.7 mmol) in pyridine (14 mL) at room temperature was added phosphorus oxychloride (0.26 mL, 2.8 mmol). After the mixture was stirred for 1 h at room temperature, the reaction was quenched at 0°C with water (10 mL). The aqueous layer was extracted with CH₂Cl₂ (10 mL x 3), and the combined organic phases were washed with brine (30 mL), dried over Na₂SO₄, filtered, and concentrated *in vacuo* to give 907 mg of white solid materials as crude products (93%). For data of 4•C₅H₅N: *Rf* values 0.20 (CH₂Cl₂/MeOH, 9:1); ¹H NMR (400 MHz, CDCl₃) 8.76 (brs, 2H, 2-positioned protons of the pyridine ring), 8.21 (dd, *J* = 7.8, 7.8 Hz, 1H, 4-positioned proton of the pyridine ring), 7.96 (d, *J* = 7.7 Hz, 1H), 7.88 (d, *J* = 7.7 Hz, 1H), 7.79–7.72 (m, 2H, 3-positioned protons of the pyridine ring), 7.65–7.61 (m, 2H), 7.45 (s, 1H), 7.42 (s, 1H), 7.18 (s, 1H), 7.16 (s, 1H), 7.12 (s, 1H), 7.10 (s, 1H), 6.55 (s, 1H), 6.42 (s, 1H), 5.76 (t, *J* = 8.0 Hz, 1H), 5.73 (d, *J* = 7.2 Hz, 1H), 5.52 (d, *J* = 7.2 Hz, 1H), 4.77 (t, *J* = 8.0 Hz, 1H), 4.69 (t, *J* = 8.0 Hz, 2H), 4.46 (d, *J* = 7.2 Hz, 1H), 4.45 (d, *J* = 7.2 Hz, 1H), 2.32–2.21 (m, 8 H), 1.47–1.27 (m, 72 H), 0.90–0.86 (m, 12 H) ppm; ¹³C NMR (100 MHz, CDCl₃) 155.9, 155.3, 155.2, 155.1 (two peaks are overlapped), 153.5, 153.4, 152.0, 151.9, 148.7, 148.3, 143.9, 143.0, 140.1, 140.0, 138.8, 138.3, 138.0, 137.7, 135.6, 135.5, 135.4, 134.3, 129.8, 129.6, 128.5, 128.4, 123.1, 122.2, 121.2, 120.4, 117.2, 117.01, 116.96, 116.8, 99.5, 99.3, 36.7, 36.5, 36.1, 34.5, 32.2 (many peaks are overlapped), 31.5, 31.3, 30.9, 30.2 (many peaks are overlapped), 30.0 (many peaks are overlapped), 29.7, 28.4, 28.3, 28.2, 23.0 (many peaks are overlapped), 14.4 (many peaks are overlapped) ppm; ³¹P NMR (162 MHz, CDCl₃) –14.7 ppm; MS (ESI) m/z : 1316 [M-C₅H₆N]⁻; IR (neat): 2922, 2851, 1487, 1269, 1160, 957, 594 cm⁻¹; HRMS (ESI) calcd. for C₈₂H₁₁₂N₂O₁₀P: 1315.8060 [M-C₅H₆N]⁻, found: 1315.8063.

Synthesis of 4

(see Scheme 2(c)) To a solution of 4•C₅H₅N (400 mg, 0.29 mmol) in CH₂Cl₂ (10 mL) was added 1 M aq. HCl (10 mL) dropwise over 1 min, and the mixture was stirred for 10 min at room temperature. The aqueous layer was

extracted with CH₂Cl₂ (10 mL x 3), and the combined organic phases were washed with 1 M aqueous HCl (10 mL x 4) and brine (20 mL), dried over Na₂SO₄, filtered, and concentrated *in vacuo* to give 350 mg of brownish white solid materials as crude products (93%). For data of **4**: *Rf* values 0.20 (CH₂Cl₂/MeOH, 9:1); ¹H NMR (400 MHz, CDCl₃) 8.00–7.95 (m, 2H), 7.67–7.61 (m, 2H), 7.39 (s, 1H), 7.26 (s, 1H), 7.23–7.20 (m, 2H), 7.16 (s, 1H), 7.11 (s, 1H), 6.58 (s, 1H), 6.43 (s, 1H), 5.79 (t, *J* = 7.7 Hz, 1H), 5.72 (d, *J* = 7.0 Hz, 1H), 5.57 (d, *J* = 7.0 Hz, 1H), 4.72–4.64 (m, 3 H), 4.42 (d, *J* = 7.0 Hz, 2H), 3.94 (brs, 1H, -OH), 2.31–2.21 (m, 8 H), 1.43–1.26 (m, 72 H), 0.89–0.86 (m, 12 H) ppm; ¹³C NMR (100 MHz, CDCl₃) 156.1, 155.8, 155.4, 155.0, 153.3, 153.2, 152.7, 152.1, 146.3 (d, *J*_{CP} = 7.9 Hz), 145.8 (d, *J*_{CP} = 7.9 Hz), 140.2 (two peaks are overlapped), 139.0, 138.1, 137.9, 137.6, 135.2, 134.8 (d, *J*_{CP} = 3.5 Hz), 133.6 (d, *J*_{CP} = 3.5 Hz), 130.0 (two peaks are overlapped), 128.6, 128.4, 123.5, 122.3, 121.8, 120.4 (two peaks are overlapped), 117.4, 117.3, 117.0 (d, *J*_{CP} = 4.2 Hz), 116.5 (d, *J*_{CP} = 4.2 Hz), 99.6, 99.4, 36.7, 36.6, 36.2, 34.6, 32.3 (many peaks are overlapped), 31.7, 31.1, 30.9, 30.1 (many peaks are overlapped), 29.8 (many peaks are overlapped), 28.4, 28.2 (many peaks are overlapped), 23.0 (many peaks are overlapped), 14.5 ppm (many peaks are overlapped) ppm; ³¹P NMR (162 MHz, CDCl₃) –14.0 ppm; MS (ESI) m/z : 1316 [M-H]⁻; IR (neat): 2922, 2851, 1487, 1331, 1158, 1005, 957 cm⁻¹; HRMS (ESI) calcd. for C₈₂H₁₁₂N₂O₁₀P: 1315.8060 [M-H]⁻, found: 1315.8030.

Representative procedure for synthesis of 6 and 7

(see Table 1, entry 10) Under an argon atmosphere, to a solution of 3•(2-vinyl)pyridine (461 mg, 0.30 mmol) in toluene (1.0 mL) at room temperature was added the stock solution of aniline (0.08 mL, 0.90 mmol) and pyrazole (61 mg, 0.90 mmol) in toluene (0.16 mL). The resultant brown solution was stirred at 45°C for 12 h, and all the starting (2-vinyl)pyridines were consumed. The reaction was quenched by addition of water (5.0 mL), and the aqueous layer was separated, which was followed by extraction with CH₂Cl₂ (10 mL x 3). The combined organic phases were washed with brine (10 mL), dried over Na₂SO₄, filtered, and concentrated *in vacuo* to give the crude products. Purification by short-plugged silica-gel column chromatography (CH₂Cl₂/EtOAc = 1/1) give 11 mg of **6** (19%) as brown oil, and **7** of 27 mg (52%) as pale brown oil. For data of **6**: *Rf* values 0.63 (CH₂Cl₂/EtOAc, 1:1); ¹H NMR (400 MHz, CDCl₃) 8.57 (dd, *J* = 4.8, 1.8 Hz, 1H), 7.60 (ddd, *J* = 7.6, 7.6, 1.8 Hz, 1H), 7.19–7.13 (m, 4 H), 6.69 (dd, *J* = 7.3, 7.3 Hz, 1H), 6.64 (d, *J* = 7.6 Hz, 2 H), 4.18 (brs, 1H), 3.54 (t, *J* = 6.6 Hz, 2 H), 3.09 (t, *J* = 6.6 Hz, 2 H) ppm; ¹³C NMR (100 MHz, CDCl₃) 160.1, 149.7, 148.5, 136.8, 129.6, 123.7, 121.8, 117.6, 113.2, 43.86, 37.78 ppm. For data of **7**: *Rf* values 0.18 (CH₂Cl₂

/EtOAc, 1:1), ^1H NMR (400 MHz, CDCl_3) 8.56 (dd, $J = 4.5$, 1.7 Hz, 1 H), 7.53 (ddd, $J = 7.6$ Hz, 7.6, 1.7 Hz, 1 H), 7.50 (d, $J = 2.0$ Hz, 1 H), 7.19 (d, $J = 2.0$ Hz, 1 H), 7.13 (dd, $J = 7.6$, 4.5 Hz, 1 H), 6.97 (d, $J = 7.6$ Hz, 1 H), 6.13 (dd, $J = 2.0$, 2.0 Hz, 1 H), 4.57 (t, $J = 7.0$ Hz, 2 H), 3.36 (t, $J = 7.0$ Hz, 2 H) ppm; ^{13}C NMR (100 MHz, CDCl_3) 158.4, 149.8, 139.7, 136.8, 129.7, 124.0, 122.0, 105.3, 51.8, 39.2 ppm; MS (DART-TOF) m/z : 174 $[\text{MH}]^+$; IR (neat): 2941, 1593, 1436, 1396, 1089, 1050, 750 cm^{-1} ; HRMS (DART-TOF) calcd. for $\text{C}_{10}\text{H}_{12}\text{N}_3$: 174.1030 $[\text{MH}]^+$, Found: 174.1032.

Representative procedure for catalytic reactions in the synthesis of **6** and **7**

(see Table 2, entry 10) Under an argon atmosphere, to a solution of **3** (29 mg, 0.02 mmol) in toluene (1.0 mL) at room temperature was added (2-vinyl)pyridine (0.11 mL, 1.0 mmol). After the mixture was stirred for 15 min, the stock solution of aniline (0.32 mL, 3.0 mmol) and pyrazole (204 mg, 3.0 mmol) in toluene (0.16 mL) was added. The resultant brown solution was stirred at 45°C for 48 h, and all the starting (2-vinyl)pyridine was consumed. After stirred for 48 h, the reaction was quenched by addition of water (5.0 mL) over 1 min at 0°C, the aqueous layer was separated and followed by extraction with CH_2Cl_2 (10 mL \times 3). The combined organic phases were washed with brine (10 mL), dried over Na_2SO_4 , filtered, and concentrated *in vacuo* to give the crude products. Purification by short-plugged silica-gel column chromatography (CH_2Cl_2 /EtOAc = 1/1) give **6** of 93 mg (47%) as brown oil, and **7** of 74 mg (43%) as pale brown oil. The samples were identical to the authentic compounds in all data.

Acknowledgments

JSPS Grant-in-Aid for Scientific Research (C), Grant Number 19K05426, which supported T.I. in this work, is gratefully acknowledged for funding. This work was supported by 2020 the Joint Research Center for Science and Technology of Ryukoku University. The authors thank Dr Toshiyuki Iwai and Dr Takatoshi Ito and Dr Seiji Watase at ORIST for gentle assistance with HRMS and crystallographic analysis. Prof. Dr Schramm, M. P. at CSULB are gratefully thanked for helpful discussions. *Dedicated to Professor François Diederich who sadly passed away on the 23rd of September 2020*

Disclosure statement

No potential conflict of interest was reported by the author(s).

Funding

This work was supported by the JSPS [19K05426].

ORCID

Tetsuo Iwasawa  <http://orcid.org/0000-0002-1068-2733>

References

- [1] (a) Diederich AF. 40 years of supramolecular chemistry. *Angew Chem Int Ed.* **2007**;46(1–2):68–69. (b) F. Diederich, *Molecular Recognition Studies with Cyclophane Receptors in Aqueous Solutions in Modern Cyclophane Chemistry*, Wiley-VCH, Weinheim, 2004; (c) F. Diederich, P. Mattei, *Helvetica Chimica Acta.* 1997, **80**, 1555–1588.
- [2] (a) Chao AY, Cram DJ. Catalysis and chiral recognition through designed complexation of transition states in transacylations of amino ester salts. *J Am Chem Soc.* **1976**; **98**. 1015–1017. (b) R. Breslow, J. B. Doherty, G. Guillot, C. Lipsey, beta-Cyclodextrinylbisimidazole, a model for ribonuclease. *J. Am. Chem. Soc.* 1978, **100**, 3227–9; (c) J. Lehn, C. Sirlin, Molecular catalysis: enhanced rates of thiolysis with high structural and chiral recognition in complexes of a reactive macrocyclic receptor molecule. *Chem. Commun.* 1978, **21**, 949–951
- [3] Christianson ADW. Structural biology and chemistry of the terpenoid cyclases. *Chem Rev.* **2006**;106:3412–3442. (b) K. M. Lancaster, M. Roemelt, P. Ettenhuber, *Science* 2011, **334**, 974–977
- [4] (a) Fersht AA. Enzyme structure and mechanism. New York:Freeman;1984. p. 47–97; (b) R. Breslow, *Artificial Enzymes*, Wiley-VCH, Weinheim, 2005
- [5] (a) Cech ATR. *Biologic catalysis by RNA in the Harvey lecture, series 82*. New York: Alan R. Liss, Inc. 123–144; (b) P. Dagenais, N. Girard, E. Bonneau, P. Legault, *Wiley Interdiscip rev RNA.* 2017, **8**, e1421
- [6] (a) Jans AACH, Caumes X, Reek JNH. Gold Catalysis in (Supra)Molecular Cages to Control Reactivity and Selectivity. *ChemCatChem.* **2019**; **11**. 287–297; (b) N. Natarajan, E. Brenner, D. Sémeril, D. Matt, J. Harrowfield, The Use of Resorcinarene Cavitands in Metal-Based Catalysis. *Eur. J. Org. Chem.* 2017, 6100–6113; (c) P. D. Frischmann, M. J. MacLachlan, Metallocavitands: an emerging class of functional multi-metallic host molecules. *Chem. Soc. Rev.* 2013, **42**, 871–890
- [7] (a) Hooley ARJ, Rebek J Jr. Chemistry and catalysis in functional cavitands. *Chem Biol.* **2009**;16(3):255–264; (b) J. Rebek Jr., *Nature* 2006, **444**, 557
- [8] Homden DM, Redshaw C. The use of calixarenes in metal-based catalysis. *Chem Rev.* **2008**;108:5086–5130.
- [9] Engeldinger E, Armspach D, Matt D. Capped cyclodextrins. *Chem Rev.* **2003**;103(11):4147–4174.
- [10] (a) Zhang D, Martinez A, Dutasta J-P. Emergence of hemicryptophanes: from synthesis to applications for recognition, molecular machines, and supramolecular catalysis. *Chem Rev.* **2017**;117:4900–4942.
- [11] (a) Moran AJR, Karbach S, Cram DJ. Cavitands: synthetic molecular vessels. *J Am Chem Soc.* **1982**;104:5826–5828; (b) P. Roncucci, L. Pirondini, G. Paderni, C. Massera, E. Dalcanale, V. A. Azov, F. Diederich, *Chem. Eur. J.* 2006, **12**, 4775–4784

- [12] Digest review, Iwasawa T. Recent developments of cavitand-recessed type metal catalysts. *Tetrahedron Lett.* **2017**;58(45):4217–4228.
- [13] (a) Endo N, Inoue M, Iwasawa T. Rational design of a metallocatalytic cavitand for regioselective hydration of specific alkynes. *Eur J Org Chem.* **2018**;2018(9):1136–1140. (b) M. Inoue, K. Ugawa, T. Maruyama, T. Iwasawa, *Eur. J. Org. Chem.* 2018, 5304–5311
- [14] Endo N, Kanaura M, Schramm MP, et al. An introverted bis-au cavitand and its catalytic dimerization of terminal alkynes. *Eur J Org Chem.* **2016**;2016(14):2514–2521.
- [15] The seminal works on phosphate and phosphonate cavitands, see, (a) Lippmann AT, Dalcanale E, Mann G. Synthesis and configurational analysis of phosphorus bridged cavitands. *Tetrahedron Lett.* **1994**;35:1685–1688. (b) T. Lippmann, H. Wilde, E. Dalcanale, L. Mavilla, G. Mann, U. Heyer, S. Spera, Synthesis and Configurational Analysis of a Novel Class of Cavitands Containing Four Dioxaphosphocin Moieties. *J. Org. Chem.* 1995, *60*, 235–242; (c) P. Delangle, J.-P. Dutasta, Tetrakisphosphonate-calix[4]resorcinarene. A powerful host for alkali metal and ammonium cations encapsulation. *Tetrahedron Lett.* 1995, *36*, 9325–9328; (d) P. Jacopozzi, E. Dalcanale, S. Spera, L. A. J. Christoffels, D. N. Reinhoudt, T. Lippmann, G. Mann, Synthesis and configurational analysis of phosphonate cavitands. *J. Chem. Soc. Perkin Trans 2.* 1998, *3*, 671–678; (e) P. Delangle, J.-C. Mulatier, B. Tinant, J.-P. Declercq, J.-P. Dutasta, Synthesis and Binding Properties of *iiii* (4i) Stereoisomers of Phosphonato Cavitands – Cooperative Effects in Cation Complexation in Organic Solvents. *Eur. J. Org. Chem.* 2001, *3*, 3695–3704; (f) B. Bibal, B. Tinant, J.-P. Declercq, J.-P. Dutasta, Preparation and Structure of *iiiiii* Tetrakisphosphonatocavitands Bearing Long Chain Functionality at the Lower Rim: Metal Picrates Extraction Studies. *Supramol. Chem.* 2003, *15*, 25–32; (g) I. Marin-Torres, G. Ogalla, J.-M. Yang, A. Rinaldi, A. M. Echavarren, Enantioselective Alkoxy cyclization of 1,6-Enynes with Gold(I)-Cavitands: Total Synthesis of Mafaicheenamine C. *Angew. Chem. Int. Ed.* 2021, *60*, 9339–9344; (h) R. Pinalli, M. Suman, E. Dalcanale, Cavitands at Work: From Molecular Recognition to Supramolecular Sensors. *Eur. J. Org. Chem.* 2004, *3*, 451–462
- [16] Castro PP, Zhao G, Masangkay GA, et al. Quinoxaline excision: a novel approach to tri- and diquinoxaline cavitands. *Org Lett.* **2004**;6:333–336.
- [17] The single crystal was prepared by slow evaporation of acetone (10 mL) solution of the sample (20 mg); CCDC-1875354: the data can be obtained free of charge from The Cambridge Crystallographic Data Centre. Triclinic, space group *P*-1, colorless, $a = 13.6025(4) \text{ \AA}$, $b = 18.7915(7) \text{ \AA}$, $c = 19.1394(7) \text{ \AA}$, $\alpha = 93.895(7)^\circ$, $\beta = 106.371(8)^\circ$, $\gamma = 105.465(7)^\circ$, $V = 4469.4(4) \text{ \AA}^3$, $Z = 2$, $T = 173 \text{ K}$, $d_{\text{calcd.}} = 1.207 \text{ g cm}^{-3}$, $\mu(\text{Mo-K}\alpha) = 0.094 \text{ mm}^{-1}$, $R_1 = 0.0914$, $wR_2 = 0.2331$, GOF = 1.012.
- [18] The corresponding spectra of ^1H NMR and ^{13}C NMR are placed in Supporting Information (Figure S1).
- [19] The ^{13}C NMR (100 MHz, CD_2Cl_2) of $1\text{-C}_5\text{H}_5\text{N}$ finds three kinds of pyridine carbon peaks located at 139.9, 138.9, 124.1 ppm for 2-, 4-, 3-positioned carbons, respectively (Figure S1).
- [20] Azov VA, Jaun B, Diederich F. NMR investigations into the vase-kite conformational switching of resorcin[4]arene cavitands. *Helv Chim Acta.* **2004**;87:449–462.
- [21] Inoue M, Kamiguchi S, Ugawa K, et al. Evaluation of the Catalytic Capability of cis- and trans- Diquinoxaline Spanned Cavitands. *Eur J Org Chem.* **2019**;36:6261–6268.
- [22] Inoue M, Fujii Y, Matsumoto Y, et al. Inherently chiral cavitand curvature: diastereoselective oxidation of tethered allylsilanes. *Eur J Org Chem.* **2019**;5862–5874. DOI: [10.1002/ejoc.201900891](https://doi.org/10.1002/ejoc.201900891)
- [23] (a) The pK_a value of diethyl phosphate is 1.39; see. Quin LD. A guide to organophosphorus chemistry. New York: Wiley. 133–165; **2000**. chap. 5; (b) J. Itoh, K. Fuchibe, T. Akiyama, *Angew. Chem. Int. Ed.* 2006, *45*, 4796–4798
- [24] Wang -Y-Y, Kanomata K, Korenaga T, et al. Enantioselective aza Michael-type addition to alkenyl benzimidazoles catalyzed by a chiral phosphoric acid. *Angew Chem Int Ed.* **2016**;55:927–931.
- [25] The free acids **1-4** made the corresponding complexes with (2-vinyl)pyridine in a molar ratio of 1:1. ^1H NMR spectra were listed in Supporting Information (Figure S2).
- [26] Kovacevic LS, Idziak C, Markevicius A, et al. Superelectrophilic amidine dications: dealkylation by triflate anion. *Angew Chem Int Ed.* **2012**;51:8516–8519.
- [27] (a) Pauling AL. Nature of forces between large molecules of biological interest*. *Nature.* **1948**;161(4097):707–709; (b) D. J. Cram, M. E. Tanner, R. Thomas, *Angew. Chem. Int. Ed.* 1991, *30*, 1024–1027; (c) J. Rebek, Jr., J. Kang, *Nature* 1997, *385*, 50–52
- [28] (a) Galan AA, Ballester P. Stabilization of reactive species by supramolecular encapsulation. *Chem Soc Rev.* **2016**;45:1720–1730; (b) J. Rebek., in *Hydrogen-bonded Capsules*, World Scientific Publishing Co. Pte Ltd., Imperial College Press, UK, 2016, pp. 191–216.
- [29] (a) Mosca AS, Yu Y, Gavette JV, et al. A Deep Cavitand Templates Lactam Formation in Water. *J Am Chem Soc.* **2015**; *137*. 14582–14583; (b) D. M. Kaphan, F. D. Toste, R. G. Bergman, K. N. Raymond, Enabling New Modes of Reactivity via Constrictive Binding in a Supramolecular-Assembly-Catalyzed Aza-Prins Cyclization. *J. Am. Chem. Soc.* 2015, *137*, 9202–9205; (c) B. Chatelet, V. Dufaud, J.-P. Dutasta, A. Martinez, Catalytic Activity of an Encaged Verkade's Superbase in a Base-Catalyzed Diels–Alder Reaction. *J. Org. Chem.* 2014, *79*, 8684–8688; (d) T. Iwasawa, R. J. Hooley, J. Rebek, Stabilization of Labile Carbonyl Addition Intermediates by a Synthetic Receptor. *Jr., Science* 2007, *317*, 493–496